

# NMR-Based Cross-Link Densities in EPDM and EPDM/ULDPE Blend Materials and Correlation with Mechanical Properties

Akshay Karekar,\* Reinhold Pommer, Bianca Prem, Caterina Czibula, Christian Teichert, Gregor Trimmel, and Kay Saalwächter\*

The role of cross-linking in dictating the microstructural and mechanical properties in ethylene-propylene-diene-monomer rubber (EPDM) and EPDM/ULDPE blends cross-linked by different sulfur amounts is investigated by solid-state  $^1\text{H}$  time-domain NMR spectroscopy and tensile-tests. Analyses of spin-spin relaxation time ( $T_2$ ), by combining free-induction decay (FID), magic-sandwich echo-FID, and Hahn-echo experiments demonstrate a reduction in crystal-amorphous interface regions of pure ultralow-density polyethylene (ULDPE) upon curative addition. The blends demonstrate a complete loss of these fractions due to curative-induced plasticization and solvation by polyethylene segments of EPDM. Cross-link densities, quantified by the magnitude of residual dipolar coupling constant ( $D_{\text{res}}$ ), arising from topological restrictions to segmental motions, are measured by multiple-quantum experiments. The entanglement-dominated EPDMs demonstrate a significant reduction in ultimate tensile properties with increasing  $D_{\text{res}}$ . The analogous blends yield similar  $D_{\text{res}}$  values up to 0.36 phr of free sulfur. Thereafter, a deviation from the cross-linking trend of the EPDMs is observed with the blends approaching a cross-linking limit, thus emphasizing the migration of additives to the amorphous phase of the ULDPE. From the additional contributions of solvation and complex entanglement scenarios in the blends, restoration and even significant enhancement in ultimate tensile strength are achieved. Limitations in applying the popular Mooney–Rivlin analysis are also briefly discussed.


## 1. Introduction

Vulcanized goods based on natural and synthetic rubbers have an enormous technological and economic importance in a range of industries.<sup>[1–4]</sup> Considering the growing diversity of applications, however, single-component materials do not often meet the various requirements. In that respect, blending of raw polymeric components has become an established and versatile method to customize material properties. Polymer blending conveniently allows the favorable features of at least two constituents to be combined and balanced. Rather than a focus on inherent properties, their synergistic effects can be used.<sup>[2,5,6]</sup> Further benefits arise from the possibility to utilize inexpensive components while maintaining a certain property profile and therefore the reduction of manufacturing costs, as well as the potential optimization of processability.<sup>[7,8]</sup>

The sustained growth and significant market share of polymer blends have been comprehensively discussed in literature.<sup>[9,10]</sup> Within these multicomponent systems, blends and composites of

A. Karekar, K. Saalwächter  
 Institut für Physik-NMR  
 Martin-Luther-Universität Halle-Wittenberg, Halle  
 Betty-Heimann-Strasse 7, Halle (Saale) 06120, Germany  
 E-mail: akshay.karekar@physik.uni-halle.de;  
 kay.saalwaechter@physik.uni-halle.de

R. Pommer, B. Prem  
 Polymer Competence Center Leoben GmbH  
 Roseggerstrasse 12, Leoben 8700, Austria  
 R. Pommer, B. Prem, G. Trimmel  
 Institute for Chemistry and Technology of Materials  
 Graz University of Technology  
 Stremayrgasse 9, Graz 8010, Austria  
 C. Czibula  
 Institute of Bioproducts and Paper Technology  
 Graz University of Technology  
 Inffeldgasse 23, Graz 8010, Austria  
 C. Czibula, C. Teichert  
 Institute of Physics  
 Montanuniversitaet Leoben  
 Franz-Josef-Strasse 18, Leoben 8700, Austria

 The ORCID identification number(s) for the author(s) of this article can be found under <https://doi.org/10.1002/mame.202100968>

© 2022 The Authors. Macromolecular Materials and Engineering published by Wiley-VCH GmbH. This is an open access article under the terms of the Creative Commons Attribution-NonCommercial License, which permits use, distribution and reproduction in any medium, provided the original work is properly cited and is not used for commercial purposes.

DOI: 10.1002/mame.202100968

synthetic rubbers and thermoplastic polyolefins are commonly used. Combinations of ethylene-propylene-diene-monomer rubber (EPDM), an amorphous elastomer of major industrial importance, with different types of semicrystalline thermoplastics, that is, polypropylene or polyethylene, have been investigated and applied for decades.<sup>[11–14]</sup> Overall physico-mechanical properties of polymer blends are evidently dependent on the chemical and structural properties of the raw components, their blending ratio, manufacturing methods, and effectively on their morphology and thermodynamic compatibility, which dictates how the components form into a fully miscible, partially miscible, or immiscible system. Here, EPDM/thermoplastic blends are typically assigned to the latter, despite some minor degree of compatibility.<sup>[6,15–17]</sup>

The macroscopic performance of the resulting materials can be conveniently evaluated by mechanical testing, by the determination of thermal properties, chemical resistance, and solubility, as well as by the measurements of electrical or optical properties by different means.<sup>[18,19]</sup> The typical rubber-elastic properties of EPDM and elastomers in general are attributed to moderate cross-linking of the soft polymer chains, which generates an insoluble network. Introducing a non-cross-linked, reinforcing and weldable thermoplastic constituent allows for a variety of improvements.<sup>[4,5,18]</sup> Explaining the origin of the synergistic effects in the polymer blend is not a trivial task, and determining its macroscopic properties only do not usually provide sufficient information. Along with the abovementioned properties, another crucial aspect lies in the type of chemical cross-linking of the material, which is sulfur-, peroxide-based, or radiation promoted, as well as in an understanding of the density and distribution of cross-links within the blend system on a molecular level.<sup>[20–22]</sup> Conventional methods to assess the segmental molecular weight include equilibrium swelling or diffusion experiments, rheological measurements, or by derivation from elasticity theory using mechanical data, such as stress-strain or dynamic-mechanical analysis.<sup>[20,23–26]</sup> All of these methods reach their limits when it comes down to a true quantification of cross-linking densities or elucidation of a phase-resolved distribution thereof.

Nuclear magnetic resonance (NMR) spectroscopy has evolved as a popular technique for elucidation of molecular information, be it structure or dynamics. The dependence of the macromolecular behavior on these molecular and microscopic origins can thus be understood using NMR techniques. Cross-link density in EPDM using different cross-linker systems has already been studied by solid-state NMR, and the role of entanglements in network properties has been established, too.<sup>[27–32]</sup>

Inclusion of thermoplastic polyolefins introduces synergistic effects now arising from the elements of crystallinity and molecular entanglements. Using NMR spectroscopy, the effects of these parameters in cross-linked EPDM/polyolefin blends have been investigated by <sup>1</sup>H lineshape analyses by spinning the blends at the magic-angle (MAS),<sup>[33]</sup> and <sup>1</sup>H-<sup>13</sup>C cross polarization-MAS experiments.<sup>[34]</sup> In a time-domain study, cross-link densities have been qualitatively analyzed by combining spin-spin relaxation time ( $T_2$ ), obtained by a free induction decay (FID), with a double-quantum (DQ) filtered Hahn-echo.<sup>[35]</sup> Despite the abundant molecular information obtained through these diverse NMR methodologies, they lack a direct quantification of the network density in the blends.

In the past couple of decades, a rather robust time-domain multiple-quantum (MQ) experiment has been used to unravel molecular details in a wide range of polymeric materials,<sup>[36]</sup> such as swollen gels,<sup>[37]</sup> nanocomposites,<sup>[38]</sup> polymer melts,<sup>[39]</sup> and rubber blends.<sup>[40]</sup> Topological constraints such as cross-links and entanglements cause a non-isotropic averaging of segmental fluctuations of the polymer chains, which leads to a residual value of the dipole-dipole interaction constant,  $D_{\text{res}}$ , among the protons on the monomers.  $D_{\text{res}}$  is an appropriate and quantitative measure of the constraint density as it has an inverse proportionality with the number of Kuhn segments between the constraints. In addition to this, the distributions of these constraints across the volume of a sample, and the amount of defects (uncoupled fractions) can also be quantified. Thus, a realistic picture of the nature of a polymer sample can be obtained.

Subject of this study is the elucidation of relative cross-linking densities in sulfur-cured EPDM samples, as well as in binary EPDM/ultralow-density polyethylene (ULDPE) blends, and to reveal the correlation of these findings with macroscopic properties. EPDM and EPDM/ULDPE blends at a fixed weight ratio of 60/40 were processed by means of a standard mixing procedure and subsequent curing by hot-press molding, using gradually increasing amounts of a sulfur-based cross-linking system. Vulcanization characteristics and mechanical properties of the obtained materials were investigated by rheological measurements and uniaxial tensile testing, respectively. Differential scanning calorimetry (DSC) was performed to investigate miscibility and thermal properties of the materials. The blend morphology was further studied by atomic force microscopy (AFM). Weakening of mechanical properties for pure EPDM samples with an increasing sulfur content can be observed, whilst surprisingly, the immiscible EPDM/ULDPE blends benefit from a rising degree of cross-linking in the rubber phase and yield significantly improved mechanical properties. Extensive studies by solid-state <sup>1</sup>H NMR experiments provide information on the phase composition of the materials, the effect of additives on the respective phases as well as the preferential distribution in those. Herein, relative cross-linking densities as function of the sulfur content in the pure elastomer samples and elastomer/thermoplastic blends are determined and the relationship with the mechanical properties is discussed.

## 2. Experimental Section

### 2.1. Materials and Sample Preparation

Amorphous EPDM (grade Keltan 6950C) with a specified ethylene content of  $44 \pm 2.1$  wt% and an ENB (ethylidene-norbornene) content of  $9.0 \pm 0.8$  wt% was supplied by LANXESS (Germany), and ultralow-density polyethylene-hexene copolymer (ULDPE, grade Attane 4607GC) was obtained by Dow Chemical Company (Midland, USA). Ground sulfur was provided by Solvay (Germany), and accelerators *N*-cyclohexyl-2-benzothiazole sulfenamide, tetramethyl thiuram disulfide (TMTD), and diphenyl guanidine were supplied by Lions Industries (Slovakia). All chemicals were used without further purification. Samples of EPDM and EPDM/ULDPE (60/40 weight ratio) were prepared by mastication and melt-blending utilizing a Plasti-Corder internal mixer (Brabender, Germany) at a mixing temperature of

140 °C and a rotor speed of 75 rpm for 5 min each. Sulfur-based cross-linking formulations with varied quantities of S (0, 0.36, 0.72, and 1.44 parts per hundred rubber, “phr”) and the accelerator mixture at a consistent quantity of 4 phr were applied to EPDM. In the EPDM/ULDPE blends, the same proportions of additives with respect to the EPDM amount were applied. Following an overnight storage of the compounds, curing agents were subsequently added to the polymer compounds on a two-roll mill (Servitec, Germany) at room temperature. Vulcanization characteristics of the prepared mixtures after overnight storage were measured using a Rheoline Multifunction moving-die rheometer (Prescott Instruments, UK) at 190 °C (timed test at constant frequency of 1.67 Hz and amplitude of 0.50° arc). The compounded rubber sheets were thereafter vulcanized at 190 °C using an electrical press (Collin, Germany). For comparative purposes, pristine EPDM (without additives, named hereafter as “E-pure”), pristine ULDPPE (without additives, named hereafter as “U-pure”), and ULDPPE with a quantity of curing agents corresponding to an EPDM/ULDPE (20/80) formulation (referred to as U-20/80) were prepared analogously by subjecting them to the same thermal history as the EPDMs and the blends.

## 2.2. Characterization Methods

### 2.2.1. Mechanical Testing

Mechanical characteristics, that is, tensile strength (TS), ultimate elongation, and moduli of rubber samples and blends were investigated using an Autograph AGS-X universal tensile tester (Shimadzu, Japan). Tests were performed on dumbbell-shaped specimens (total length = 100 mm, clamping length = 75 mm, width = 3 mm) at a tensile rate of 500 mm min<sup>-1</sup> without preload. Sample thickness was determined by means of a Digimatic Micrometer (Mitutoyo, Japan).

### 2.2.2. Differential Scanning Calorimetry

DSC measurements were performed utilizing a DSC 214 Polyma (Netzsch, Germany). Heat flow curves were recorded from –120 to 300 °C at a heating rate of 10 K min<sup>-1</sup> in N<sub>2</sub> atmosphere. Glass transition and melting temperatures were defined by inflection and peak point values, respectively.

### 2.2.3. Atomic Force Microscopy

AFM was applied to study the morphology and phase separation of the samples. For this purpose, cross-sectional samples of cross-linked EPDM and EPDM/ULDPE blends were prepared by cryo-microtomy cutting. All AFM measurements were recorded in tapping mode using an Asylum Research MFP-3D AFM (Santa Barbara, CA, USA). The instrument was equipped with a closed-loop planar x-y-scanner with a scanning range of 85 × 85 μm<sup>2</sup> and a z-range of 15 μm. As AFM probes, standard silicon probes (Olympus AC160TS, Japan) were employed which had a cantilever spring constant of about 30 N m<sup>-1</sup> and a tip radius of about 15 nm. The measurements were obtained in intermittent

contact mode under ambient conditions at 46 ± 9% relative humidity and a temperature of 23 ± 1 °C. Topography and phase images were recorded at three independent positions for each sample. Phase imaging can be used to obtain a qualitative material contrast.<sup>[41,42]</sup> The data was processed in the open-source software Gwyddion.<sup>[43]</sup>

### 2.2.4. Solid-State Time-Domain <sup>1</sup>H NMR Spectroscopy

<sup>1</sup>H NMR measurements of the cured series of EPDM and EPDM/ULDPE blends were performed on a Bruker minispec mq 20 benchtop spectrometer (20 MHz proton resonance frequency) having a 90° pulse length of 2.6 μs and a dead time of 12 μs. The samples, stacked to a height of 6 mm in an NMR tube having a diameter of 10 mm, were measured under air at 70 °C using a BVT 3000 temperature controller.

## 2.3. NMR Theory

### 2.3.1. Decomposition of Polymer Fractions by T<sub>2</sub> Relaxometry

Study of transverse magnetization decay by an FID gives information on polymer relaxation at short evolution times. Depending on the nature of the decay and by using a suitable fitting function,<sup>[44–52]</sup> fractions associated with different T<sub>2</sub> relaxation times in the polymer can be classified. In the current setup, fractions with relaxation time scales up to 0.2 ms can be easily classified, beyond which magnetic field heterogeneities dominate. To probe somewhat mobile fractions (associated with longer relaxation time scales), Hahn-echo T<sub>2</sub> relaxometry is used. Thus, by stitching data obtained from FID and Hahn-echo, the gamut of different relaxation time scales and the corresponding quantities of the fractions can be extracted.<sup>[53]</sup> In NMR phenomenology, protons in shorter chain segments (higher cross-linking) relax faster (⇒ shorter T<sub>2</sub>) than segments in longer network chains (⇒ longer T<sub>2</sub>).

Limitations arise when probing rigid fractions, such as chain segments that are part of the crystallites, as in the case of ULDPPE. These correspond to a rigid limit coupling constant of about 30 kHz, with time scale of relaxation of about 20 μs. Due to the inevitable receiver dead time, precious information is lost in the early part of an FID decay. To compensate for this signal loss in the short-time limit, an echo experiment like the pulsed version of the magic-sandwich echo (MSE) is used.<sup>[54]</sup> MSE performs a time-reversal of the decay signal by refocusing multispin dipolar interactions. Figure A (see Appendix) gives a perspective highlighting the loss of initial signal in an FID due to the highly constrained fractions in pure ULDPPE. Also demonstrated is the signal compensation achieved by an MSE using a short interpulse delay (τ<sub>φ,MSE</sub>) of 2 μs. Hence, by simultaneous fitting of the Hahn-echo-extended FID with MSE-FID using a multicomponent modified-exponential decay function (∝ f<sub>x</sub> exp[-(t/T<sub>2,x</sub><sup>eff</sup>)<sup>β<sub>x</sub></sup>]), a complete description of polymer relaxation can be obtained.<sup>[53]</sup> An effective T<sub>2</sub> (T<sub>2</sub><sup>eff</sup>) is obtained in the presence of dipolar couplings. The rigid crystallites are described by a shape parameter, β = 2 (Gaussian decay), and lower values of β are obtained due to coupling distributions and relaxation

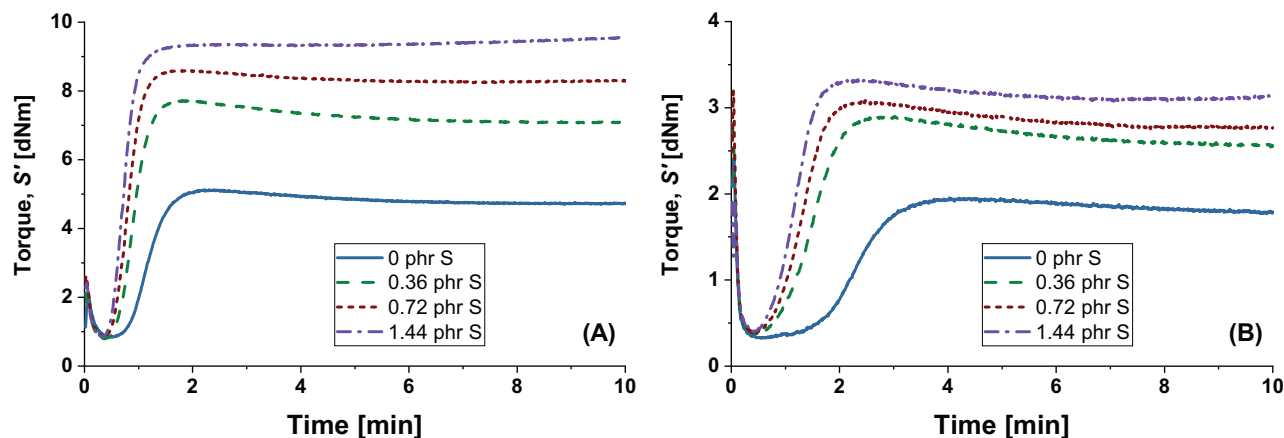


**Figure 1.** Vulcanization curves at a curing temperature of 190 °C for A) EPDM compounds, and B) EPDM/ULDPE blends, both with varied concentrations of elemental sulfur (0, 0.36, 0.72, and 1.44 phr S).

effects. The different fractions,  $f_x$ , corresponding to the different relaxation times can be thus obtained from such a fit.

### 2.3.2. Time-Domain MQ NMR Measurements for Elucidation of Cross-Link Densities

As for the degree of cross-linking, it is reflected in the residual dipolar coupling constant extracted from the MQ NMR data introduced earlier. It is directly proportional to the segmental dynamic order parameter,  $S_b$ , and thus inversely proportional to the Kuhn segments of the polymer chains. To obtain an absolute value of the cross-link density, certain model considerations are necessary for the polymer of interest.<sup>[55]</sup> Since this value is unknown for EPDM, a relative  $D_{\text{res}}$  description would suffice.

The used MQ pulse sequence,<sup>[36]</sup> based on the works of Baum and Pines,<sup>[56]</sup> gives a DQ build-up signal ( $I_{\text{DQ}}$ ) arising due to contributions from coupled spins, which decays at longer DQ evolution times. Additionally, a decaying reference signal ( $I_{\text{ref}}$ ), comprising of contributions from coupled and also uncoupled spins (defects) is used for normalization by point-by-point division of the DQ signal. Presence of isotropically active mobile defects (consisting of mechanically irrelevant fractions of chain ends, loops and sol) are accounted for by subtracting them during normalizations. An adequate subtraction of the decay “tail” results in the normalized DQ signal,  $I_{\text{nDQ}}$ , reaching a 0.5 intensity limit. The  $I_{\text{nDQ}}$  signal can be fitted using a fitting function that uses an Abragam-like kernel function, which describes the rise of the nDQ intensity in terms of  $D_{\text{res}}$ ,<sup>[57]</sup> combined with a numerically calculated integral over a log-normal coupling distribution:<sup>[58]</sup>

$$P(\ln(D_{\text{res}})) = \frac{1}{\sigma_{\ln} \sqrt{2\pi}} \exp \left[ -\frac{\{\ln(D_{\text{res}}) - \ln(D_{\text{med}})\}^2}{2\sigma_{\ln}^2} \right] \quad (1)$$

The fitting parameters are thus the median value  $D_{\text{med}}$  as well as the logarithmic standard deviation  $\sigma_{\ln}$ . The latter is positive and dimensionless and reflects the distribution full width at half maximum roughly in the unit of decades (e.g.,  $\sigma_{\ln} = 0.5$  corresponds

to a half-decade wide distribution). For an entanglement-rich polymer such as EPDM, the total measured coupling strength,

$$D_{\text{res}} \propto \frac{1}{M_{c, \text{EPDM}}} + \frac{1}{M_{e, \text{EPDM}}} \quad (2)$$

wherein  $M_c$  is the average molecular weight between cross-links and  $M_e$  is the average entanglement molecular weight.

## 3. Results and Discussion

### 3.1. Curing Characteristics

First, the vulcanization behaviors of the compounds were studied using a moving-die rheometer. Rheological curves at 190 °C for EPDM and EPDM/ULDPE (60/40) compounds with four different quantities of elemental sulfur recorded at preset strain and frequency are shown in **Figure 1**. It must be noted that all formulations contain equal amounts of sulfur-donating accelerator components (TMTD). This method allows to follow the progress of the vulcanization process by measuring the elastic torque ( $S'$ ), as the material's resistance to shear deformation increases with the formation of cross-links in the system. EPDM compounds with free sulfur (0.36 to 1.44 phr S) exhibit very similar and sharp vulcanization onset times and subsequently reach plateaus, which expectedly show higher maximum torques for higher sulfur contents. Increasing torques can therefore be used as indication for an increase of the relative cross-linking densities in the system.<sup>[24–26,59]</sup> Comparable observations regarding the vulcanization onset can be made for EPDM/ULDPE blends. Owing to the thermoplastic content in the mixture, the measured torque is significantly lower, and the curing period appears slightly broadened. Again, the steadily growing peak torque values in dependence on the sulfur loading indicate a higher degree of vulcanization. This applied curing formulation in combination with extended vulcanization times generally creates a network with predominantly short cross-links (esp. mono- and di-sulfide linkages) and a comparably low portion of polysulfide links.<sup>[60,61]</sup>

Regarding the formulations without free sulfur (0 phr S), which essentially rely on the sulfur released from the donating

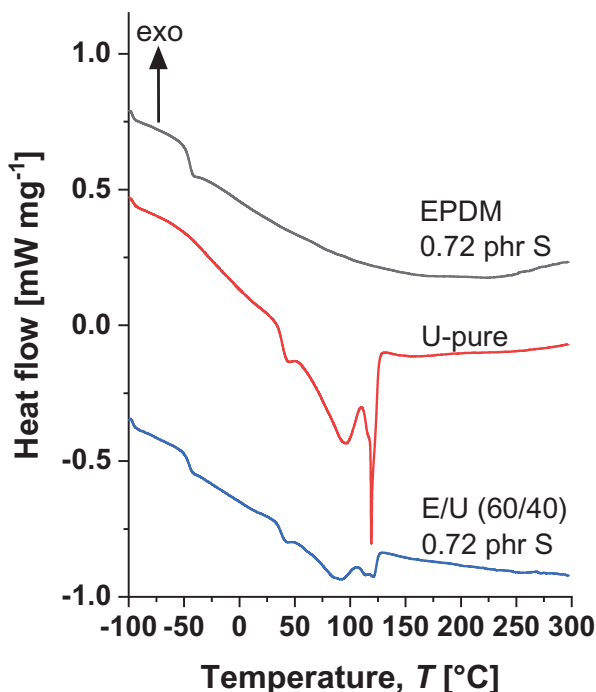


**Figure 2.** DSC curves for pure ULDPE (U-pure), and cross-linked EPDM and EPDM/ULDPE blend with 0.72 phr sulfur. Shown here are the first melting cycles measured at a temperature ramp rate of 10 K min<sup>-1</sup>.

vulcanization agent TMTD, a prolonged scorch time is evident for both, the rubber and the rubber/thermoplastic blend systems. This is attributed to the delayed availability of sulfur provided by the decomposition process of the thiuram compound. In this case, using sulfur-donating agents only, a stable vulcanization network with a comparably very high content of mono- and di-sulfide links is formed.<sup>[61,62]</sup> All samples were consistently prepared by hot press molding for 10 min at 190 °C.

### 3.2. Semicrystalline Morphology

DSC and AFM were used to analyze the effect of blending on the semicrystalline properties of the blends. DSC was on the one hand performed to investigate the thermal properties of the single materials, and on the other hand, to obtain information on the thermodynamic compatibility or miscibility of polymers in the blend system. Representative DSC curves for molded samples during the first heating cycle at a temperature ramp rate of 10 K min<sup>-1</sup> are presented in **Figure 2**. The glass transition temperature  $T_g$  of the vulcanized EPDM (0.72 phr S) compound was found to be -44 °C. The pure ULDPE shows a  $T_g$  at 38 °C and a rather broad melting range  $T_m$  with two distinct peaks at 96 °C and 119 °C. As for the EPDM/ULDPE (60/40) blend (0.72 phr S), a  $T_{g,1}$  is measured at -46 °C which is assigned to the rubber phase. A further  $T_{g,2}$  of 39 °C along with the broad melting range (with considerably less distinct, yet recognizable peaks at ≈92 °C and a double peak at 114–121 °C) are attributed to the ULDPE phase. Comparing the thermal transition temperatures in the blend and the respective single materials, only a negligible shift of the values can be observed. This suggests that the

EPDM/ULDPE blend represents an immiscible system at lower temperatures.

To get a better insight on the phase separation and illustrate its complexity, AFM topography scans with corresponding phase images have been obtained on microtomed cross sections of cross-linked EPDM and the EPDM/ULDPE (60/40) blend, both containing 0.72 phr free sulfur (**Figure 3**). In Figures 3A and 3B, topography images (acquired in intermittent contact mode) of the EPDM sample and the blend are presented, respectively. The corresponding phase images have been recorded for the EPDM sample (**Figure 3C**) in attractive mode with a phase angle larger than 90° and for the EPDM/ULDPE (60/40) blend in repulsive mode with phase angle <90° (see **Figure 3D**). Since EPDM is softer than ULDPE, the phase contrast between both materials is quite strong in **Figure 3D**. The darker color corresponds to a low phase angle and indicates the ULDPE domains, whereas the brighter color corresponds to a high phase angle and characterizes the softer EPDM matrix. The phases are rather randomly distributed in the EPDM/ULDPE blend and the phase separation length between the individual phases is roughly in the range of 0.1–0.5 μm. The ULDPE phase is characterized by spherical structures with about 0.1–0.2 μm diameter, which frequently coalesce to larger regions of 0.5 μm. Sometimes, even continuous random networks of connected ULDPE areas are observed. However, possible influences from sample preparation and migration effects cannot be completely excluded. Therefore, one should be careful to directly relate the AFM information to the actual bulk morphology.

### 3.3. Mechanical Properties

Improving the mechanical properties is one of the key reasons for blending elastomeric and thermoplastic materials. Systems combining rubbers and different grades of polyethylene have reportedly shown benefits for tensile, ageing, or abrasion properties.<sup>[5,63,64]</sup> As already stated, within this study the effect of different quantities of vulcanization agents was investigated.

By standardized uniaxial tensile testing, the TS and elongation at break (EB) of the samples were determined, which constitute essential material characteristics. **Figure 4A** compares the TS and EB for cross-linked EPDM samples. Here, the sample cured with 0 phr elemental sulfur demonstrates superior TS and EB of ≈9 MPa and >1000%, respectively. A significant drop of both TS and elongation can be observed by introducing free sulfur (specimen with 0.36 phr S) as a vulcanization agent and therefore creating a denser cross-linking network with greater rigidity. A higher sulfur content leads to a subsequent but comparably less rapid decrease, effectively yielding a TS of 1.9 MPa and an EB of 240% at a sulfur loading of 1.44 phr S. The mechanical properties are apparently strongly dependent upon the distribution, density, and length of the sulfur cross-links, which reportedly can be varied by means of the sulfur quantity added to the rubber compounds.<sup>[2,20,22]</sup> EPDM/ULDPE (60/40) samples, which are presented in **Figure 4B** demonstrate a contrary effect, which reveals superior tensile properties of the elastomer/thermoplastic blends and the reinforcing nature of the ULDPE component. By a stepwise increase of the sulfur content, the system shows an improved TS of up to 24 MPa, along with rather comparable

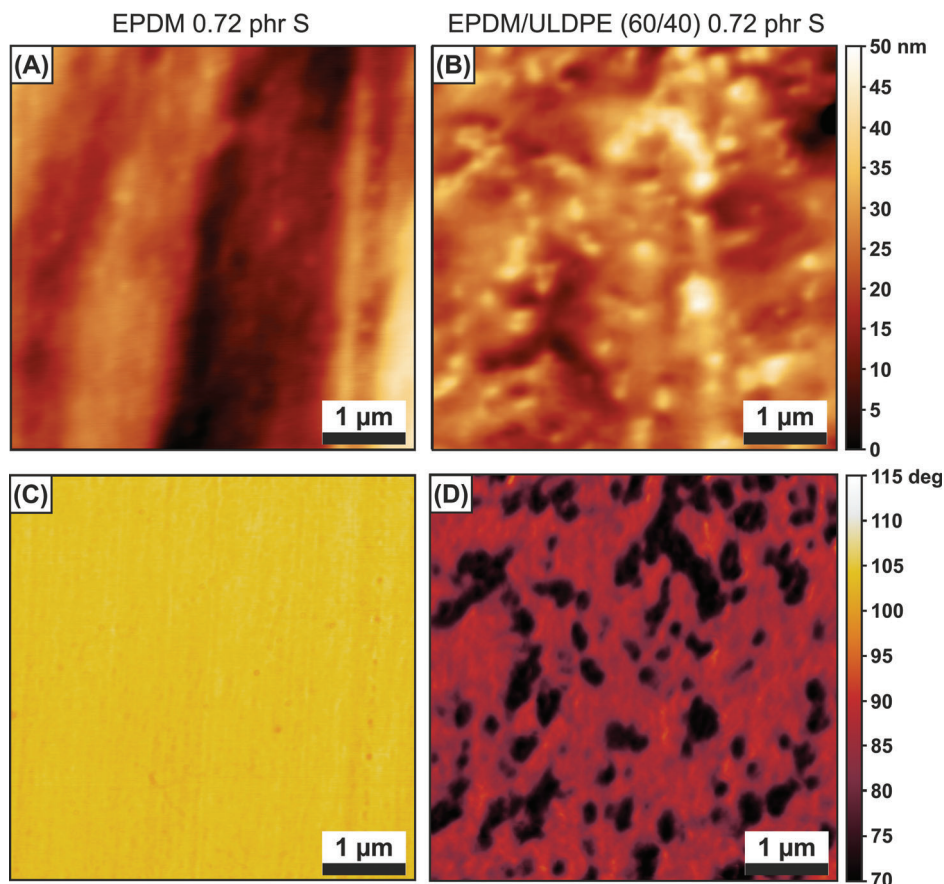


**Figure 3.**  $5 \times 5 \mu\text{m}^2$  A,B) AFM topography images and C,D) corresponding phase images for A,C) cross-linked EPDM, and B,D) cross-linked EPDM/ULDPE (60/40) blend, both containing 0.72 phr free sulfur. The dark areas in (D) indicate the harder ULDPE phase.

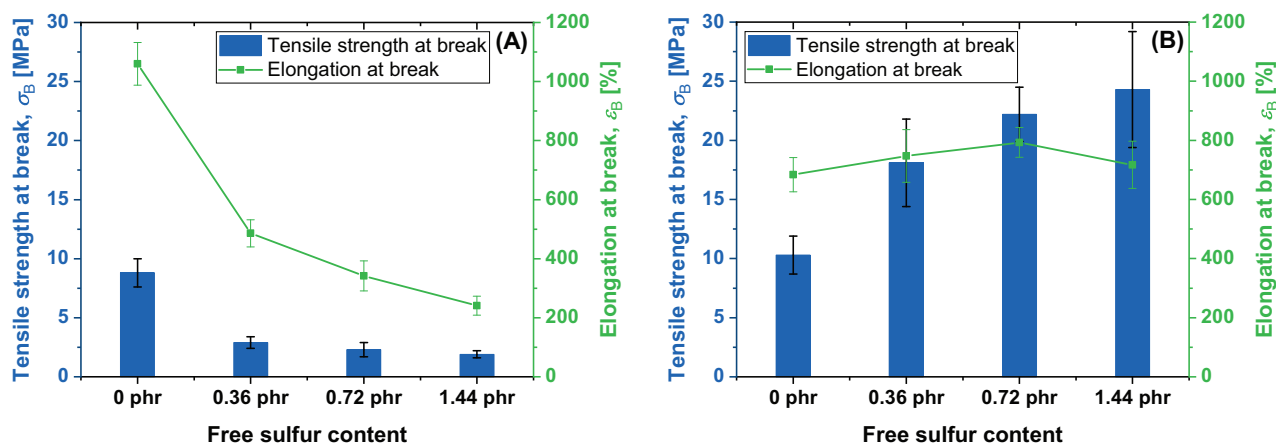


**Figure 4.** Comparison of tensile strength at break and elongation at break for A) EPDM compounds, and B) EPDM/ULDPE blends, both with varied concentrations of elemental sulfur (0, 0.36, 0.72, and 1.44 phr S).

mean elongations at break between about 700% and 800%. **Table 1** summarizes the results of the tensile tests. For reference, pure ULDPE (U-pure) was processed and tested analogously. Additionally, a sample of ULDPE containing vulcanization agents (U-20/80) was analyzed in order to see a potential influence of the vulcanization agents on the mechanical properties, as well as

on the phase composition determined via NMR characterization. Mechanical properties of these samples are also included in **Table 1**.

The reinforcing role of ULDPE within the rubber/thermoplastic system is further emphasized by comparing the stress–strain curves of the EPDM/ULDPE blend with

**Table 1.** Summary of tensile strength (TS) and elongation at break (EB) values for all investigated samples with varied formulations.

EPDM	TS [MPa]	EB [%]
0 phr S	8.8 ± 1.2	1060 ± 72
0.36 phr S	2.9 ± 0.5	486 ± 46
0.72 phr S	2.3 ± 0.6	342 ± 51
1.44 phr S	1.9 ± 0.3	241 ± 32
EPDM/ULDPE (60/40)	TS [MPa]	EB [%]
0 phr S	10.3 ± 1.6	684 ± 58
0.36 phr S	18.1 ± 3.7	747 ± 89
0.72 phr S	22.2 ± 2.3	793 ± 50
1.44 phr S	24.3 ± 4.9	717 ± 80
ULDPE	TS [MPa]	EB [%]
U-pure <sup>a)</sup>	27.8 ± 1.8	602 ± 20
U-20/80 <sup>b)</sup>	27.6 ± 2.0	610 ± 24

<sup>a)</sup> ULDPE without any additives; <sup>b)</sup> ULDPE processed with a quantity of cross-linking agents corresponding to an EPDM/ULDPE (20/80) blend formulation.

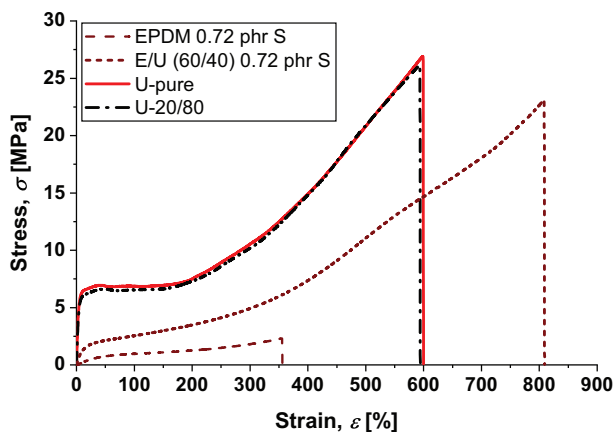


**Figure 5.** Representative stress–strain curves of EPDM as well as EPDM/ULDPE (60/40) cured with 0.72 phr S, and processed U-pure and U-20/80.

the respective single materials (Figure 5). Herein, the blend (0.72 phr S) does not only show superior mechanical features when compared to EPDM (0.72 phr S), but also clearly improved values of EB relative to pure ULDPE samples which were processed in the same way. The addition of vulcanization agents to ULDPE has no obvious impact on the macroscopic mechanical properties, neither on TS, EB, nor on the progression of the stress–strain curve. Likewise, the linear-regime modulus is also identical ( $\approx 150$  MPa) for both the ULDPE variants. In case of the blends, the Young’s modulus is obtained to be about 10.5 MPa across all the sulfur compositions. It is hence remarkable to note that despite being much softer, at high cross-linking, the blend has virtually the same ultimate properties as pure ULDPE.

In order to correlate mechanical properties with results from cross-linking density determination, measured stress–strain curve relations were further used to calculate moduli of the

materials. Whilst for EPDM/ULDPE samples the distinct linear elastic region allowed for the direct determination of the Young’s modulus, this method appeared inadequate for the EPDM samples. Therefore, an evaluation based on the Mooney–Rivlin (MR) model was chosen.<sup>[65,66]</sup> For assessment of the apparent Mooney–Rivlin constants ( $2C_1$  and  $2C_2$ ), which are assigned to the cross-link modulus ( $G_c$ ) and entanglement modulus ( $G_e$ ), respectively, the reduced stress ( $\sigma_{\text{red}}$ ) is plotted against the reciprocal deformation ( $\lambda^{-1}$ ), according to Equation (3).

$$\sigma_{\text{red}} = \frac{\sigma}{\lambda - \lambda^{-2}} = 2C_1 + \frac{2C_2}{\lambda} \quad (3)$$

where  $\sigma_{\text{red}}$  is the reduced stress or Mooney stress,  $\lambda$  is the deformation ( $L/L_0$ ), and  $2C_1$  and  $2C_2$  are the MR constants.

Such a plot is shown in Figure 6A for an EPDM sample at 0.72 phr loading of sulfur. However, to fit such a plot it is optimum to account for errors related to the testing itself. Thus, a small correction to the deformation component as  $\lambda \pm \Delta\lambda$  can yield a linearized “corrected” reduced stress ( $\sigma_{\text{red,corr}}$ ) curve in the limit up to  $1/\lambda_{\text{corr}} = 1$ .<sup>[65]</sup> Applying a linear fitting function in the range of  $1.25 < \lambda \pm \Delta\lambda < 2.5$  ( $0.8 > \lambda \pm \Delta\lambda^{-1} > 0.4$ ), which also avoids the upturn due to finite extensibility at large strains, numerical values for  $2C_1$  and  $2C_2$  are thus determined, which are tabulated in Table 2.

The measure of cross-link density from the intercept ( $2C_1$ ) shows an expected increase in values with an increase in sulfur, as seen from  $G_c$  for the EPDMs. Contrary to the  $G_c$  trend, the apparent entanglement modulus is found to decrease slightly with increasing sulfur. Consequently, this results in the total modulus ( $G_c + G_e$ ) varying insignificantly with respect to the added free sulfur. This behavior of the entanglement modulus is an unusual finding which requires molecular-level investigations and is thus deferred to the end of the paper.

In contrast to a characteristic neo-Hookean behavior demonstrated by the EPDMs, pure ULDPE and the representative blend in Figure 6B show a deviation from this behavior. The sharp departure from linearity in the quick rise for  $1/\lambda \rightarrow 1$  even upon  $\Delta\lambda$ -correction is due to yielding in polyethylene. The retention of higher strength even after breakdown of the crystalline framework in ULDPE appears to be delayed in the blend, which probably leads to larger break-stress upon cross-linker increment even at larger strains. This could be due to a non-trivial interaction of ULDPE with the other phase (EPDM), and probably also the additives which appear to enhance the ultimate properties by dilution (discussed later).

### 3.4. Distinction of Crystalline, Amorphous, and Crystalline-Amorphous Interface Fractions in EPDM/ULDPE Blends by $T_2$ Relaxation Analyses

FID and Hahn-echo experiments serve as good tools for distinguishing the different  $T_2$ -related fractions in a polymer sample. Owing to their compositions, one can expect different relaxation patterns for the samples under study. Typical FIDs extended by respective Hahn-echo decay curves for pure EPDM, pure ULDPE, and their 60/40 blend at 0.72 phr sulfur loading are represented in Figure 7 (open symbols). The trends of these curves thus highlight their different relaxation behaviors. Also

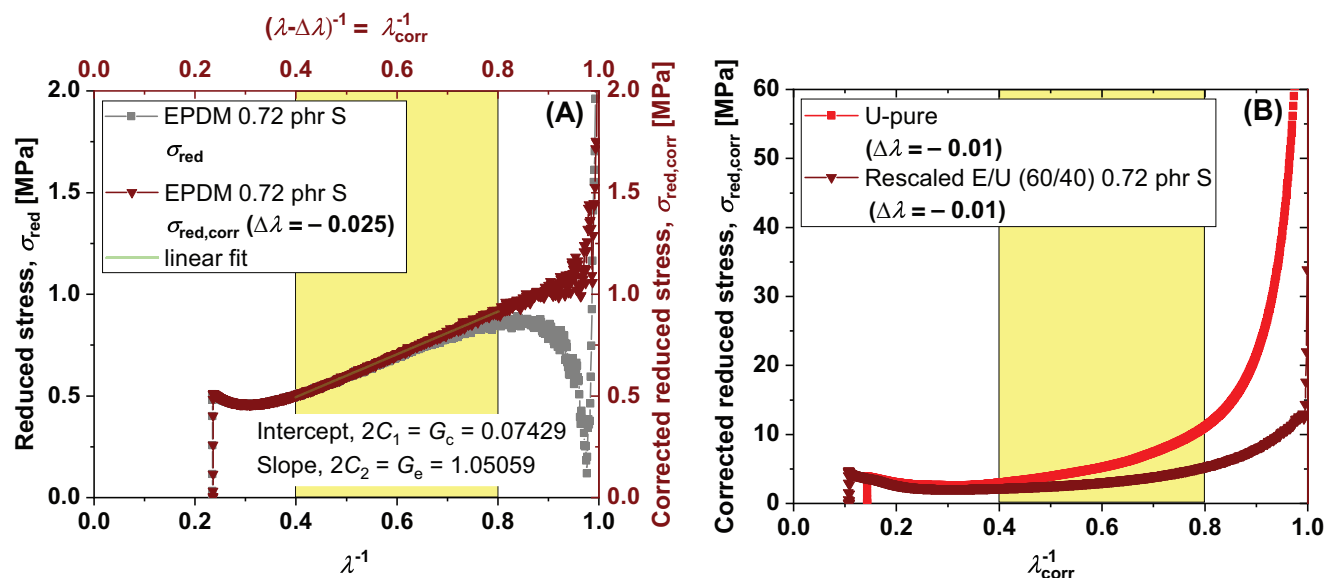


**Figure 6.** A) Exemplary plot of reduced stress against the reciprocal deformation, and the corrected reduced stress against the reciprocal corrected deformation, with a linear fit in the limits  $1.25 < \lambda - \Delta\lambda < 2.5$  ( $\Delta\lambda = -0.025$ ) according to the Mooney–Rivlin model. B) Corrected reduced stress plots of pure ULDPE and a (vertically rescaled) blend (0.72 phr S). Delayed strain-softening in the blend probably leads to enhanced strain-at-break. The sharp upturn (sharp decrease for  $1/\lambda_{corr} < 1$ ) due to yielding in polyethylene renders MR fits unusable for such materials.

**Table 2.** Young's moduli as well as results from the Mooney–Rivlin hyperelastic model for cross-linked EPDMs.

EPDM	Young's modulus [MPa]	$G_c^a$ [MPa]	$G_e^b$ [MPa]	$(G_c + G_e)$ [MPa]
0 phr S	$2.5 \pm 0.1$	-0.08	1.14	1.06
0.36 phr S	$2.3 \pm 0.1$	-0.02	1.10	1.08
0.72 phr S	$2.2 \pm 0.1$	0.07	1.04	1.11
1.44 phr S	$2.3 \pm 0.1$	0.19	0.90	1.09

<sup>a)</sup> Cross-link modulus; <sup>b)</sup> Entanglement modulus.

shown are the MSE-FIDs (solid symbols) to probe the fractions associated with very short transverse relaxation times. Simultaneous fits to the two data sets were first performed for pure EPDM (without cross-linker) using a three-component fitting function. A weighting of 10% was applied to the FID part due to the higher number of data points. The shape parameters ( $\beta_r$  and  $\beta_{m2}$ ) for the most rigid fraction ( $f_r$ ) and the most mobile fraction ( $f_{m2}$ ) were fixed to 2 and 0.8 (stretched exponential), respectively. This yielded a  $T_{2,m2}^{eff} = 1.6$  ms with the corresponding fraction,  $f_{m2} = 37\%$ . From the fit, a major fraction ( $f_{m1} \approx 63\%$ ) with  $T_{2,m1}^{eff}$  of about 0.8 ms and the corresponding value of the shape parameter ( $\beta_{m1} = 1.3$ ) were also obtained. Due to the absence of any motion-constrained components in the sample, the fit showed no indications of the presence of a rigid fraction. Here, it must be emphasized that the two mobile fractions cannot be objectively distinguished due to the rather small separation in their relaxation times. They thus represent the more or less constrained ends of a broader distribution. Due to the negligible amount of rigid fraction, a two-component fit including a built-in distribution would suffice for this particular polymer. Nevertheless, a

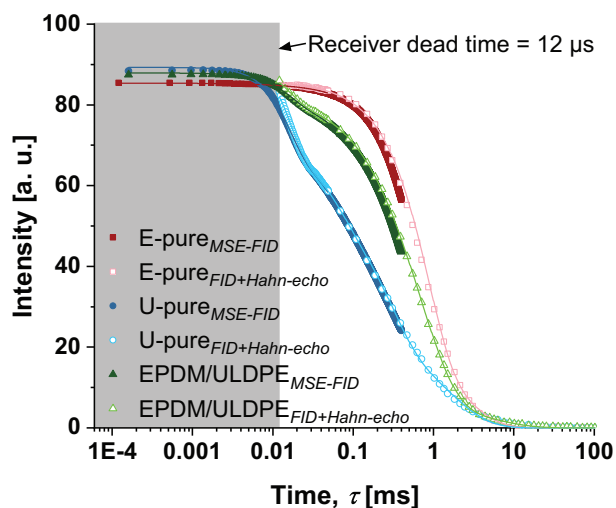


**Figure 7.** Simultaneous fits to MSE-FID with Hahn-echo-extended FID distinguishing the different relaxation patterns in various compositions. The fits are represented as solid lines for pure EPDM (three-component), pure ULDPE (four-component), and EPDM/ULDPE blend with 0.72 phr sulfur (four-component). The MSE-FIDs are fitted only until the corresponding evolution times of the FIDs ( $\approx 40 \mu$ s).

three-component fitting function (consisting of  $\beta_r = 2$ ) is essential to account for the fast relaxations of segments in crystal lamellae of ULDPE in the blends and to distinguish the contributions of EPDM fractions in the blends. Further, due to the presence of a distribution of spin–spin relaxation time constants,  $\beta_{m2}$  is restricted to a minimal value of 0.8 to avoid the ambiguity that a too-stretched exponential “steals away” amplitude from a close by  $T_2$  component. Note that the two components used to describe the



**Table 3.** Rigid fractions in the polyethylene homopolymer variants and EPDM/ULDPE blends.

	U-pure	U-20/80	Blends
$f_c$ [%]	24.0	24.0	9.5
$f_{ci}$ [%]	14.0	9.0	0

long-time contribution do not correspond to physically distinguishable components; rather, the two-component fit just serves to parameterize the data and allow for a comparison among the samples.

Unlike the amorphous EPDM, the presence of crystalline regions in ULDPPE contributes also to shorter relaxation times. Thus, a four-component fitting function is suitable to probe pure ULDPPE and the blends. For pure ULDPPE, the fit yielded a rigid fraction amounting to 24% of the sample. This fraction, having a Gaussian decay ( $\beta = 2.0$ ) with a  $T_2^{eff}$  of about 16  $\mu\text{s}$ , can be attributed to the crystalline lamellae ( $f_c$ ). A second fraction of 14%, associated with a transverse relaxation time of 65  $\mu\text{s}$  and  $\beta = 1.5$ , was also obtained. Fractions with these relaxation times are associated with semirigid regions of intermediate motions, which in a semicrystalline polymer are the interfaces between crystalline lamellae and the amorphous regions (hence referred as  $f_{ci}$ ).<sup>[35]</sup> In comparison, U-20/80 (not shown in the figure) has a similar quantity of  $f_c$ , suggesting that the amount of crystalline regions remain unchanged (Table 3). Fascinatingly though, the intermediate regions dropped down to about 9%. This is a rather surprising outcome, and could probably be due to a plasticizing effect of the additives included in the polymer which seem to interfere at the crystallite-amorphous interface regions. An account of the fitting uncertainty in these systems by multicomponent modified-exponential decay function is given in the Supporting Information.

To have a comparative consistency between the samples, the shape parameters and the  $T_2^{eff}$  relaxation times of  $f_c$  and  $f_{ci}$  for U-20/80 were kept consistent with the values obtained through fitting pure ULDPPE. The same protocol was employed for the blends too. The representative plot in Figure 7 demonstrates the changes arising in the sample due to blending. Figure 8 provides an overview of the soft EPDM-related fit fractions ( $\Rightarrow$  m1 and m2) in the blends. These are compared with the fit components having similar spin-spin relaxation times in the polyethylene variants. The loss in the intermediate fractions of U-20/80 reflects as a gain in its amorphous  $f_{m1}$  fraction. However, no evidence of these microscopic changes can be inferred in the stress-strain curve in Figure 5.

In the blend, upon addition of the accelerator mixture, a jump of 30% in  $f_{m1}$  can be seen which can be attributed to the formation of cross-links in the EPDM phases. Here, it is important to note that  $f_{m1}$  also contains polyethylene segments constrained by entanglements and linkage to the crystals in the amorphous regions of ULDPPE. Upon addition of free sulfur to the subsequent blends, one may expect a measurable change in the fit components related to m1 fractions. Surprisingly though, no apparent change in  $f_{m1}$  can be observed, but only a small decrease in the subsequent  $T_{2,m1}^{eff}$ . This probably suggests that the blends are approaching a cross-linking limit. The most mobile frac-

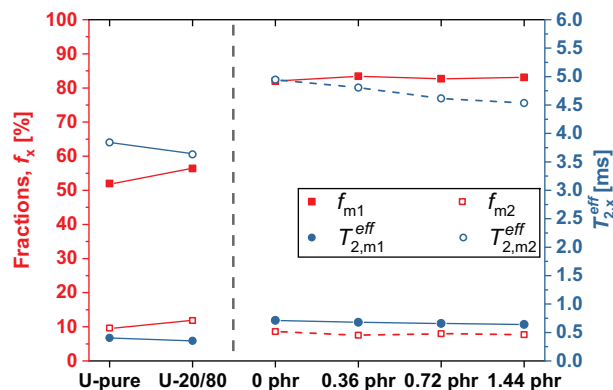


**Figure 8.** EPDM-related fit components in the blends compared with fit components of similar  $T_2$  in pure ULDPPE (U-pure) obtained from a four-component fit. Also shown is U-20/80 for comparison. The lines are a guide to the eye only. For discussion pertaining to crystalline and intermediate fractions, see text.

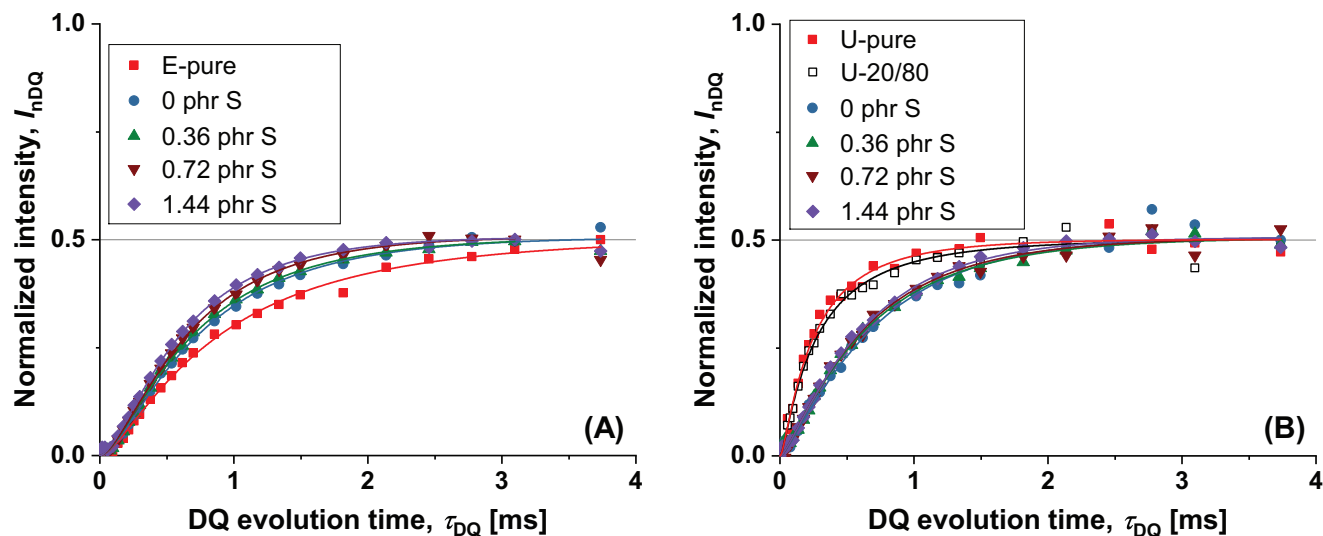
tion ( $f_{m2}$ ) has low-to-no change between the polyethylenes and the blends, suggesting that these fractions are unaffected by the cross-links.

Table 3 contains a summary of the results from the crystalline and intermediate fractions. The crystalline fractions remained constant at about 9.5% for all the blends, which scales with the weighted amount of ULDPPE in the blends. Interestingly though, no evidence of fractions with intermediate motions can be observed in the blends, either due to the additives interfering with the crystal-amorphous interfaces (as witnessed in U-20/80) or polyethylene regions of EPDM interacting with the ULDPPE phases or both. The latter factor may be supported by the finding that largely similar relaxation times are obtained for the amorphous regions of ULDPPE and EPDM pertaining fractions in the blends ( $f_{m1}$  and  $f_{m2}$ ) at any given cross-linker amount (Figure 8). Thus, one may expect a miscibility of amorphous ULDPPE with the chemically similar EPDM phase. Elsewhere, X-ray studies have demonstrated the solvation of LDPE by ethylene termonomers present in EPDM in peroxide vulcanized EPDM/LDPE blends.<sup>[67]</sup> The solvation has been attributed to interfere with the crystalline phases in LDPE. In a follow-up research, the blend composition has been observed to affect the overall degree of crystallinity and the morphology of the crystalline phases too.<sup>[68]</sup> However, in the present study, the most constrained fractions (crystalline phases,  $f_c$ ) have been measured to be almost equal to the weighted average of the rigid fraction in pure ULDPPE. It may thus be deduced that the solvation, in the samples discussed here, does not interfere with the crystallization and hence, occurs only at the interfaces.

The changes in EPDM upon cross-linking are better understood through  $D_{res}$  studies. Hence, these samples will be dealt in the next section with MQ experiments.

### 3.5. Cross-Linking in EPDM and EPDM/ULDPE Blends

Cross-linking leads to restrictions in chain motions due to the arising constraints. Additionally, depending on various factors like cross-linker system, processing conditions, presence of



**Figure 9.** Normalized DQ build-up curves for A) EPDM, and B) EPDM/ULDPE (60/40) blends at different cross-linker levels. DQ curves of E-pure, U-pure, and U-20/80 are plotted for comparison. A bimodal fitting function is used for the blends to separately account for ULDPE and EPDM phases (see text for explanation), whereas a single-mode fitting function is sufficient for the EPDMs. The fits are represented as solid lines, while the fit results are summarized in Figure 10.

fillers, and the polymer itself, finite amounts of isotropically relaxing defects are also generated due to imperfect cross-linking reactions. These were quantified by fitting an exponential decay fitting function to the difference signal ( $I_{\text{ref}} - I_{\text{DQ}}$ ) to achieve an optimum normalized DQ build-up signal. The cross-linked EPDMs possess a single defect fraction (average  $T_2 \approx 5.5$  ms), which amounted to  $\approx 7\%$  in the lowly cross-linked sample and reduced to  $\approx 3\%$  in the sample with 1.44 phr sulfur. In the blends, in addition to the defects from EPDM, a rather slowly relaxing defect component (average  $T_2 \approx 13.5$  ms) was also obtained. The total defect fraction in the blends reduced from  $\approx 18\%$  for the blend without free sulfur to  $\approx 10\%$  in the highly cross-linked sample, the additional defect fraction coming from the unconstrained chain segments in ULDPE phase.

The normalized DQ build-up curves obtained after the normalization for the different EPDM samples are plotted in **Figure 9A**. The  $D_{\text{res}}$  is reflected in the slope of the curves in the initial region. A somewhat high  $D_{\text{res}}$  value of 0.240 kHz for uncross-linked EPDM suggests the presence of strong entanglement-related effects in the terpolymer. It thus becomes apparent that in this case  $D_{\text{res}} \approx 1/M_{\text{e,EPDM}}$  only. A comparably wide  $D_{\text{res}}$  distribution ( $\sigma_{\text{in}} = 0.862$ ) is obtained for uncross-linked EPDM, which is a manifestation of the inherent spin-heterogeneity due to the different constituent monomers. In the cross-linked samples, as can be expected, the cross-link density increases with the addition of the fixed amount of accelerator mixture and the increasing free sulfur, and thus follows the  $D_{\text{res}}$  description given in Equation (2). It may be necessary to remind oneself that the trends of build-up curves seen here are originating only due to the modifications of unsaturations present in the ENB fractions of the terpolymer. The ethylene and propylene segments would remain chemically inert. Additionally, the inherently present entanglements can also get trapped upon cross-linking and contribute to the overall  $D_{\text{res}}$ .<sup>[31]</sup> This effect can

become profound when norbornene rings are trapped at such junctions.

MQ experiments on samples with ULDPE (**Figure 9B**) were performed by applying a MAPE (Magic And Polarization Echo) filter to the Baum–Pines pulse sequence discussed above.<sup>[69]</sup> Such a  $T_2^{\text{eff}}$ -filter, effectively an “artificially ineffective” MSE sequence, can be used to remove contributions from highly coupled spins, like those coming from the crystallites. This, thus, enables probing only the signals from cross-linked and entangled chains. For the samples discussed here, the MAPE interpulse delay ( $\tau_{\phi, \text{MAPE}}$ ) was set to 50  $\mu\text{s}$ , just sufficient to remove the effects of the crystalline regions (see **Figure A** for a qualitative description of an FID with a MAPE filter at different interpulse delays). Thus, the obtained signals will be a sum of the intermediate and amorphous regions. After such a procedure, pure ULDPE yielded a  $D_{\text{med}}$  of 0.840 kHz and a coupling distribution width of 1.01. Analogous to the reduced intermediate fractions ( $f_{\text{ci}}$ ) in U-20/80, a reduced  $D_{\text{med}}$  of about 0.760 kHz, and a comparable  $\sigma_{\text{in}}$  of 1.08 were obtained, further highlighting plasticization in ULDPE due to the additives (see Section 2.3.2 for details on the fitting parameters).

To separately account for the ULDPE and EPDM phases in the blends, the fitting function was modified to a bimodal type. Here, the values of  $D_{\text{res}}$  and its distribution obtained from pure ULDPE were attributed to the first mode in the new fit. To this, a weighting factor corresponding to the amount of ULDPE in the blends, and the exact quantity of active regions in ULDPE contributing to  $D_{\text{res}}$  was also applied during fitting. Here, the active regions are those that are remaining after subtracting the fractions lost to the interpulse delay of 50  $\mu\text{s}$  ( $\approx 40\%$ ) and defect fraction ( $\approx 10\%$ ). Thus, the resulting values of  $D_{\text{res}}$  and the distribution for the second mode will be those coming from the cross-links and entanglements in EPDM, and tie molecules and entanglements from amorphous (am) regions in ULDPE, thus modifying

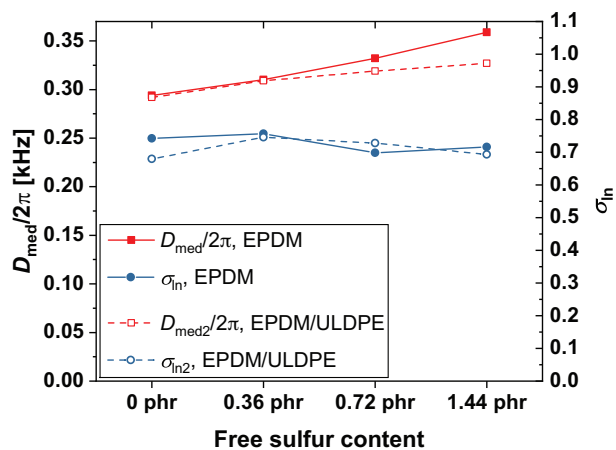


**Figure 10.** Residual dipolar coupling constants and their distributions at different sulfur concentrations for the second fitting mode ( $D_{med2}$  and  $\sigma_{in2}$ ) in blends. Discussions pertaining to the first mode can be found in the text. The results of EPDM at different sulfur concentrations have been juxtaposed here for comparison.

Equation (2) to:

$$D_{res} \propto f_{EPDM} \left( \frac{1}{M_{c, EPDM}} + \frac{1}{M_{e, EPDM}} \right) + f_{ULDPE, am} \left( \frac{1}{M_{tie, ULDPE}} + \frac{1}{M_{e, ULDPE}} \right) \quad (4)$$

where  $f_{EPDM} = 1 - f_{ULDPE, am}$  are the fractions of the detected signal. **Figure 10** summarizes and emphasizes the trends of residual dipolar coupling constants and their distributions in cross-linked EPDMs and the blends, obtained by fits to the build-up curves depicted in Figure 9. First, from the coupling distribution widths in the cross-linked EPDMs, it can be inferred that the accelerator mixture and sulfur concentration do not affect the distribution of cross-links in comparison to the inherent heterogeneity of the spin system in the EPDM terpolymer. The same observation has been made in EPDM cured by peroxides,<sup>[31]</sup> where side reactions are known to increase the overall cross-linking distribution. Approximately similar distributions are obtained in the blends too, which is an outcome of the same monomer (ethylene) being present in both the phases.

The residual dipolar coupling constants and the coupling distributions corresponding to the second mode ( $D_{med2}$  and  $\sigma_{in2}$ , respectively) are plotted in Figure 10 for the blends. As can be expected, the  $D_{res}$  gradually increases with the amount of cross-linker in the samples. The same magnitude of cross-link density is obtained for the blend and EPDM at 0 and 0.36 phr of free sulfur. However, upon further sulfur addition, a distinct deviation in the trends of cross-link densities is observed. A noticeable increase is obtained for EPDMs whereas the blends appear to approach a plateau. This complements the stagnating trend of  $f_{m1}$  discussed for the blends above. Given that the corresponding EPDM-to-curative ratios in the single vulcanizates and the blends remain the same, the flattening may again indicate migration of the curatives to the ULDPE phases of the blends, thus limiting the cross-linking in EPDM phases. Additionally, the significant role of entanglements in the blends (as a contributing factor in

Equation (4)) cannot be discounted, which probably dominates the bulk properties.

### 3.6. Facets of Reinforcement in EPDM/ULDPE Blends

Entanglements certainly appear to play a dominating role in dictating the mechanical performance in EPDM. The presence of these entanglements complements the larger strain-at-break values for the lower cross-linked variants observed in Figure 4A. The chains undergo stretching to a higher degree due to the presence of lesser permanent junctions and more mobile entanglements. As more cross-links are formed, the reduced stretchability leads to insufficient load transfers across the network and, hence, to an early failure. Thus, the sulfur bonds form the weak links.

The observed migration of curatives that lead to a decrease in crystal-amorphous interfaces in U-20/80 and a complete loss in the blends indicates a plasticization of the semicrystalline structure, thus improving their resistance to deformation by strain-hardening (See Table 1 and Figure 5). The effects of entanglements appear to be compounded in the blends, as seen in Figure 4B. An increase in tensile stress by more than twofold between 0 and 1.44 phr free sulfur appears to be a synergistic outcome of several microstructural factors. First, apart from the characteristic load-bearing by a partly continuous rigid thermoplastic embedded in the rubber matrix that leads to retention of properties to a greater extent, the hardness of the largely continuous EPDM matrix possibly dictates the efficiency of load distributions. The mechanical superiority of the blend might come into its own when ULDPE is part of a harder EPDM matrix. Interfacial failures may occur if the EPDM is too soft.

Second, the solvation of ULDPE at the crystal interface by EPDM, as remarked earlier, is another major factor in determining the blends' properties. The dedicated mixing step at 140 °C enhances homopolymer-terpolymer blending, whereby complex interactions of the highly branched ULDPE with EPDM at the thermoplastic-rubber phase boundaries can lead to different entanglement situations.

Apart from the already established dilution of the crystal-amorphous interface regions, curatives can also be localized in the blend interphases. With the addition of higher amounts of sulfur, the cross-linking at the phase boundaries can increase, and also eventually lead to improved mechanical properties. This complements the flattening of  $D_{med2}$  due to the migration of the additives away from the EPDM phase as seen in Figure 10. Lastly, the contributions of entanglement, wherein trapping of the long ULDPE branches, tie molecules, and norbornenes due to cross-linking is possible, cannot be downplayed for their role in improving the ultimate properties.

The role of entanglements, however, appears to be discounted from the empirical value of the slope ( $2C_2$ ) in the Mooney-Rivlin equation for the systems considered here, where the entanglement modulus ( $G_e$ ) shows a decreasing trend for the cross-linked EPDMs. This is in stark contrast to the NMR observations (MQ, as well as amorphous fractions in Figure 8) where the entanglements are expected to be constant, or even slightly increase with increasing cross-linker.<sup>[65]</sup> A similar trend has been observed earlier in EPDM containing about 5% ENB cross-linked

by peroxide.<sup>[31]</sup> In both instances, the decline in apparent entanglement contribution has been attributed to network inhomogeneities. This suggests that the MR approach to isolate the entanglement contribution simply fails qualitatively. Nevertheless, a direct correlation of the cross-link modulus ( $G_c$ ) to the cross-link densities with the NMR measurements for EPDMs was still possible. But again, for obtaining  $G_c$  from the polyethylene variants and the blends considered herewith, a modification of the Mooney–Rivlin equation or development of new models seems necessary.

#### 4. Conclusion

Despite decades of investigations on EPDM/polyethylene blends, the basis for certain material properties remains unclear and underappreciated. Through this study, the contrasting mechanical behaviors of sulfur cross-linked EPDM and EPDM/ULDPE blends were elucidated by solid-state  $^1\text{H}$  NMR spectroscopy. MQ NMR and  $T_2$  relaxometry studies of pure EPDM reveal the existence of a highly entanglement-dominated environment. Though cross-link density increased with the amount of cross-linker, as found qualitatively from the Mooney–Rivlin model and quantitatively by MQ NMR, it contributed only negatively toward the mechanical properties. While superior tensile stress and strain were obtained for lowly cross-linked EPDM, these properties reduced drastically with an increase in the number of cross-links, possibly due to weaker sulfur bonds.

Insights into ULDPE and EPDM/ULDPE blends proved to be particularly interesting. Where an accurate distinction and quantification of crystalline, amorphous, and crystal-amorphous regions in ULDPE was possible by NMR experiments, the crystal-amorphous regions appeared to be diluted by the inclusion of accelerator and sulfur in a ULDPE homopolymer sample. Fascinatingly, the blends demonstrated a near-complete loss of these regions, possibly also due to solvation of ULDPE by ethylene monomers present in EPDM, in addition to the already-observed dilution by additives. The amount of crystalline fractions, however, remained unchanged across these samples.

MQ measurements proved that EPDM/ULDPE blends cross-link to the same extent as EPDM up to 0.36 phr of free sulfur. Thereafter, a divergence in the cross-link density trends was observed, wherein the blends seemed to approach a constant value. A primary reason for this could be the tendency of the cross-linking system migrating to the ULDPE phase and the blend interphase, and thus starving the EPDM phase. The significant entanglement scenario in the blends from EPDM and ULDPE phases may also dominate with the addition of cross-linker.

Along with the load-bearing feature of ULDPE, inherently dominant entanglement density in the blends, solvation by EPDM, plasticization of the crystal-amorphous interface by the curatives, and possible cross-linking at the interphase leading to trapped entanglements, the samples demonstrated strain hardening. This resulted in successively improved ultimate TS in the blends, without compromising the ultimate strain across the samples. Contrary to NMR, the phenomenological Mooney–Rivlin model failed to provide a logical explanation for the role of entanglements in cross-linked EPDMs, and was also rendered unusable for ULDPE and the blends which are dominated by the modulus of the polyethylene crystallites and undergo yielding.

#### Appendix

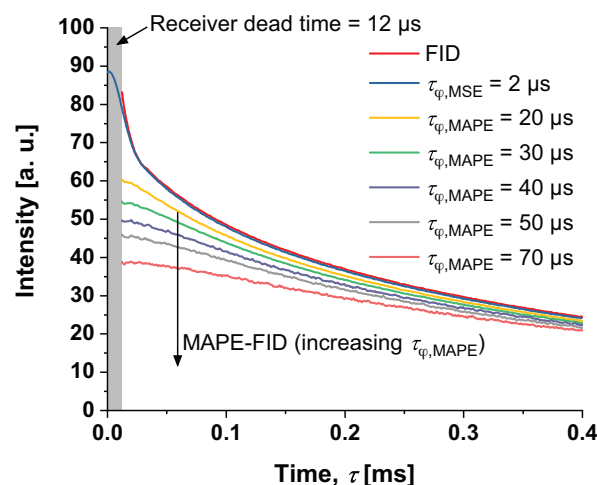


**Figure A.** An MSE-FID demonstrating signal refocusing in comparison to initial signal loss in an FID for pure ULDPE. The removal of the crystalline fractions-related signal using a MAPE filter at different interpulse delays is also demonstrated here for an FID.

#### Supporting Information

Supporting Information is available from the Wiley Online Library or from the author.

#### Acknowledgements

Parts of the research work were performed at the Polymer Competence Center Leoben GmbH (PCCL, Austria) within the framework of the COMET-program of the Federal Ministry for Climate Action, Environment, Energy, Mobility, Innovation and Technology and the Federal Ministry for Digital and Economic Affairs with contributions by Graz University of Technology, Austria (Institute of Chemistry and Technology of Materials). The PCCL is funded by the Austrian Government and the State Governments of Styria, Lower Austria and Upper Austria. A.K. thanks the Land Sachsen-Anhalt and the European Social Fund (ESF) for the grant ZS/2016/08/80644.

Open access funding enabled and organized by Projekt DEAL.

#### Conflict of Interest

The authors declare no conflict of interest.

#### Data Availability Statement

The data that support the findings of this study are available from the corresponding author upon reasonable request.

#### Keywords

cross-link densities, residual dipolar coupling constants, rubber/thermoplastic blends

Received: December 15, 2021  
Revised: January 28, 2022  
Published online:

- [1] L. A. Utracki, P. Mukhopadhyay, R. K. Gupta, in *Polymer Blends Handbook*, Vol. 1, 2nd ed. (Eds: L. A. Utracki, C. A. Wilkie), Springer, Dordrecht **2014**, Ch. 1.
- [2] W. Hofmann, *Rubber Technology Handbook*, Hanser Publishers, Munich **1989**.
- [3] Y. Hirata, H. Kondo, Y. Ozawa, in *Chemistry, Manufacture and Applications of Natural Rubber* (Eds: S. Kohjiya, Y. Ikeda), Elsevier/Woodhead Publishing, Amsterdam **2014**, Ch. 12.
- [4] F. Röthemeyer, F. Sommer, in *Kautschuk-Technologie: Werkstoffe – Verarbeitung – Produkte*, 3rd ed. (Eds: F. Röthemeyer, F. Sommer), Hanser, Munich **2013**, Ch. 1.
- [5] S. F. Xavier, in *Polymer Blends Handbook*, Vol. 2, 2nd ed. (Eds: L. A. Utracki, C. A. Wilkie), Springer, Dordrecht **2014**, Ch. 10.
- [6] L. M. Robeson, *Polymer Blends: A Comprehensive Review*, Hanser, Munich **2007**.
- [7] L. A. Utracki, G. Z.-H. Shi, D. Rodrigue, R. Gonzalez-Núñez, in *Polymer Blends Handbook*, Vol. 1, 2nd ed. (Eds: L. A. Utracki, C. A. Wilkie), Springer, Dordrecht **2014**, Ch. 9.
- [8] M. N. Subramanian, *Polymer Blends and Composites: Chemistry and Technology*, 1st ed., Wiley-Scrivener, Hoboken, NJ **2017**.
- [9] L. A. Utracki, *Commercial Polymer Blends*, Springer US, Boston, MA **1998**.
- [10] L. Robeson, *Polymers* **2014**, 6, 1251.
- [11] I. Fortelný, J. Kovář, A. Sikora, D. Hlavatá, Z. Kruliš, Z. Nováková, Z. Pelzbauer, P. Čefelín, *Angew. Makromol. Chem.* **1985**, 132, 111.
- [12] C. S. Ha, D. J. Ihm, S. C. Kim, *J. Appl. Polym. Sci.* **1986**, 32, 6281.
- [13] Z. Bartczak, A. S. Argon, R. E. Cohen, M. Weinberg, *Polymer* **1999**, 40, 2331.
- [14] C. Cazan, A. Duta, in *Advances in Elastomers I*, Vol. 11 (Eds: P. M. Visakh, S. Thomas, A. K. Chandra, A. P. Mathew), Springer, Berlin, Heidelberg **2013**, Ch. 7.
- [15] C. M. Roland, in *Advances in Elastomers I*, Vol. 11 (Eds: P. M. Visakh, S. Thomas, A. K. Chandra, A. P. Mathew), Springer, Berlin, Heidelberg **2013**, Ch. 6.
- [16] H. Veenstra, P. C. Verkooijen, B. J. van Lent, J. van Dam, A. P. de Boer, A. P. H. Nijhof, *Polymer* **2000**, 41, 1817.
- [17] B. Pukánszky, F. Tüdös, *Makromol. Chem., Macromol. Symp.* **1990**, 38, 221.
- [18] D. Campbell, R. A. Pethrick, J. R. White, *Polymer Characterization: Physical Techniques*, 2nd ed., CRC Press, Cheltenham **2000**.
- [19] *Polymer Testing*, 2nd ed. (Eds: S. Seidler, V. Alstädt, W. Grellmann), Hanser, Munich **2013**.
- [20] O. Chaikumpollert, Y. Yamamoto, K. Suchiva, S. Kawahara, *Polym. J.* **2012**, 44, 772.
- [21] F. Zhao, W. Bi, S. Zhao, *J. Macromol. Sci., Part B: Phys.* **2011**, 50, 1460.
- [22] D. Y. Kim, J. W. Park, D. Y. Lee, K. H. Seo, *Polymers* **2020**, 12, 1.
- [23] Y. H. Zang, R. Muller, D. Froelich, *Polymer* **1989**, 30, 2060.
- [24] F. A.-E. Salam, M. H. A.-E. Salam, M. T. Mostafa, M. R. Nagy, M. I. Mohamed, *J. Appl. Polym. Sci.* **2003**, 90, 1539.
- [25] Y. Shangguan, J. Yang, Q. Zheng, *RSC Adv.* **2017**, 7, 15978.
- [26] W. Chassé, M. Lang, J.-U. Sommer, K. Saalwächter, *Macromolecules* **2011**, 45, 899.
- [27] V. M. Litvinov, W. Barendswaard, M. Van Duin, *Rubber Chem. Technol.* **1998**, 71, 105.
- [28] R. A. Orza, P. C. M. M. Magusin, V. M. Litvinov, M. Van Duin, M. A. J. Michels, *Macromol. Symp.* **2005**, 230, 144.
- [29] R. A. Orza, P. C. M. M. Magusin, V. M. Litvinov, M. Van Duin, M. A. J. Michels, *Macromolecules* **2007**, 40, 8999.
- [30] P. C. M. M. Magusin, R. A. Orza, V. M. Litvinov, M. Van Duin, K. Saalwächter, *ACS Symp. Ser.* **2011**, 1077, 207.
- [31] T. Saleesung, D. Reichert, K. Saalwächter, C. Sirisinha, *Polymer* **2015**, 56, 309.
- [32] T. Saleesung, P. Saeoui, C. Sirisinha, *J. Appl. Polym. Sci.* **2017**, 134, 44523.
- [33] M. D. Ellul, A. H. Tsou, W. Hu, *Polymer* **2004**, 45, 3351.
- [34] M. Aluas, C. Filip, *Solid State Nucl. Magn. Reson.* **2005**, 27, 165.
- [35] V. M. Litvinov, *Macromolecules* **2006**, 39, 8727.
- [36] K. Saalwächter, P. Ziegler, O. Spycykerelle, B. Haidar, A. Vidal, J.-U. Sommer, *J. Chem. Phys.* **2003**, 119, 3468.
- [37] K. Saalwächter, *J. Am. Chem. Soc.* **2003**, 125, 14684.
- [38] J. Carretero-González, J. L. Valentín, M. Arroyo, K. Saalwächter, M. A. Lopez-Manchado, *Eur. Polym. J.* **2008**, 44, 3493.
- [39] F. V. Chávez, K. Saalwächter, *Phys. Rev. Lett.* **2010**, 104, 198305.
- [40] M. K. Dibbanti, M. Mauri, L. Mauri, G. Medaglia, R. Simonutti, *J. Appl. Polym. Sci.* **2015**, 132, 42700.
- [41] R. García, R. Pérez, *Surf. Sci. Rep.* **2002**, 47, 197.
- [42] S. N. Magonov, V. Elings, M.-H. Whangbo, *Surf. Sci.* **1997**, 375, L385.
- [43] D. Nečas, P. Klapetek, *Cent. Eur. J. Phys.* **2012**, 10, 181.
- [44] J. P. Cohen-Addad, *Polymer* **1983**, 24, 1128.
- [45] H. Tanaka, Y. Inoue, *Polym. Int.* **1993**, 31, 9.
- [46] D. Dadayli, R. K. Harris, A. M. Kenwright, B. J. Say, M. M. Sünnetçioğlu, *Polymer* **1994**, 35, 4083.
- [47] M. Knörger, U. Heuert, H. Schneider, P. Barth, W. Kuhn, *Polym. Bull.* **1997**, 38, 101.
- [48] E. W. Hansen, P. E. Kristiansen, P. Bjørn, *J. Phys. Chem. B* **1998**, 102, 5444.
- [49] L. Dujourdy, J. P. Bazile, J. P. Cohen-Addad, *Polym. Int.* **1999**, 48, 558.
- [50] P. E. Kristiansen, E. W. Hansen, P. Bjørn, *J. Phys. Chem. B* **1999**, 103, 3552.
- [51] S. Schreurs, J.-P. François, P. Adriaensens, J. Gelan, *J. Phys. Chem. B* **1999**, 103, 1393.
- [52] M. Knörger, U. Heuert, H. Schneider, G. Heinrich, *J. Macromol. Sci., Part B: Phys.* **1999**, 38, 1009.
- [53] A. Wittmer, R. Wellen, K. Saalwächter, K. Koschek, *Polymer* **2018**, 151, 125.
- [54] A. Maus, C. Hertlein, K. Saalwächter, *Macromol. Chem. Phys.* **2006**, 207, 1150.
- [55] K. Saalwächter, *Prog. Nucl. Magn. Reson. Spectrosc.* **2007**, 51, 1.
- [56] J. Baum, A. Pines, *J. Am. Chem. Soc.* **1986**, 108, 7447.
- [57] W. Chassé, J. L. Valentín, G. D. Genesky, C. Cohen, K. Saalwächter, *J. Chem. Phys.* **2011**, 134, 044907.
- [58] L. Jakisch, M. Garaleh, M. Schäfer, A. Mordvinkin, K. Saalwächter, F. Böhme, *Macromol. Chem. Phys.* **2018**, 219, 1700327.
- [59] C. W. Macosko, *Rheology: Principles, Measurements, and Applications*, Wiley-VCH, New York **1994**.
- [60] J. Kruželák, R. Sýkora, I. Hudec, *Chem. Pap.* **2016**, 70, 1533.
- [61] S. Howse, C. Porter, T. Mengistu, I. Petrov, R. J. Pazur, *Rubber Chem. Technol.* **2019**, 92, 513.
- [62] M. H. S. Gradwell, D. Grooff, *J. Appl. Polym. Sci.* **2002**, 83, 1119.
- [63] V. Tanrattanakul, W. Udomkichecha, *J. Appl. Polym. Sci.* **2001**, 82, 650.
- [64] H. Yao, J. Niu, J. Zhang, N. Ning, X. Yang, M. Tian, X. Sun, L. Zhang, S. Yan, *Chin. J. Polym. Sci.* **2016**, 34, 820.
- [65] S. Schlögl, M.-L. Trutschel, W. Chassé, G. Riess, K. Saalwächter, *Macromolecules* **2014**, 47, 2759.
- [66] I. Syed, G. Hempel, K. Saalwächter, P. Stratmann, M. Klüppel, *Macromolecules* **2016**, 49, 9004.
- [67] L. Ślusarski, D. Bieliński, A. Włochowicz, C. Ślusarczyk, *Polym. Int.* **1995**, 36, 261.
- [68] D. Bieliński, A. Włochowicz, J. Dryzek, C. Ślusarczyk, *Compos. Interfaces* **2001**, 8, 1.
- [69] A. Papon, K. Saalwächter, K. Schäler, L. Guy, F. Lequeux, H. Montes, *Macromolecules* **2011**, 44, 913.